

SHORT COMMUNICATION

On the *in silico* application of the center-of-mass distance method

Done Stojanov*

Department of Computer Technologies and Intelligent Systems, Faculty of Computer Science, Goce Delcev University, Stip, North Macedonia

Abstract

This study aims to protocolize the utilization of the center-of-mass (CoM) distance method in GROMACS MD simulation software as a useful method for evaluating the binding affinity change in heterodimeric protein due to induced changes in one of the units. The hypothesis underlines the basic principles in biophysics, that an increase of the binding affinity is expected to reduce the relative CoM distance between monomers, while the opposite is expected to increase the relative CoM distance. However, it has been found that the CoM distance analysis must be strictly preformed during the convergent phase of systems' dynamics, once the monomers enter mutually stable conformation — a limitation which has usually been overlooked. The method was used to study the impact of *K417Y* severe acute respiratory syndrome coronavirus 2 (SARS-CoV-2) surface glycoprotein (S-protein) mutation. It has been found that the *K417Y* mutation favors reduced binding affinity between SARS-CoV-2 S-protein and human angiotensin-converting enzyme 2 (hACE2) receptor, which is due to the loss of the permanent K417-D30 salt bridge in favor of a temporary Y417-D30 hydrogen bond. The destabilizing impact of *K417Y* mutation on S-protein–hACE2 complex was confirmed by radius of gyration analysis.

*Corresponding author:

Done Stojanov
 (done.stojanov@ugd.edu.mk)

Citation: Stojanov D. On the *in silico* application of the center-of-mass distance method. *Gene Protein Dis.* 2024;3(1):2657.
<https://doi.org/10.36922/gpd.2657>

Received: January 6, 2024

Accepted: February 29, 2024

Published Online: March 15, 2024

Copyright: © 2024 Author(s). This is an Open-Access article distributed under the terms of the Creative Commons Attribution License, permitting distribution, and reproduction in any medium, provided the original work is properly cited.

Publisher's Note: AccScience Publishing remains neutral with regard to jurisdictional claims in published maps and institutional affiliations.

Keywords: GROMACS; Simulation; Center-of-mass; Distance; *K417Y* mutation; SARS-CoV-2

1. Introduction

The center-of-mass (CoM) distance method can be formally defined as a time continuous analysis of the distance between the CoM of two structures, which constitute together a common system of interest, such as monomers in heterodimer,¹ protein-ligand complex,² or a pair of key residues.³

The core definition of the CoM distance method has been applied in several *in silico* studies.²⁻⁵ Ibrahim *et al.*,² compared inhibitor activity of erylosides B and lopinavir against severe acute respiratory syndrome coronavirus 2 (SARS-CoV-2) main protease, using molecular dynamics (MD) simulations in addition to generalized born surface area binding energy calculations. MM/GBSA (molecular mechanics with generalized Born and surface area solvation) is used as a method to snapshot the free energy of the biding between ligands (erylosides B and lopinavir, specifically) to the SARS-CoV-2 main protease, which involves MD simulations with an explicit water solvent of the protein-ligand complex.⁶ One of the methods used to show that erylosides B exhibits higher inhibitor activity against SARS-CoV-2 main protease than lopinavir is the CoM

distance. The conclusion was derived by measuring the average of the CoM distance between the ligands and SARS-CoV-2 main protease, during the course of 100-ns MD simulation. The average of the CoM distance for erylosides B was less than the average CoM distance for lopinavir, which was taken as a clue that erylosides B binds the SARS-CoV-2 main protease more effectively than lopinavir, demonstrating higher inhibitory potential.

Kumar *et al.*³ analyzed pi-stacking interaction between Omicron receptor binding domain (RBD) Tyr501 and human angiotensin-converting enzyme 2 (hACE2) Tyr41, as N501Y is one of the key mutations responsible for increased infectivity.^{1,7,8} The CoM distance between the aromatic rings has been measured, which in the case of pi-stacking interaction should not exceed 5 Å.⁹ Such interaction is going to increase hACE2-surface glycoprotein (S-protein) binding affinity that will ultimately increase infectivity. The average CoM distance between aromatic rings of <5 Å in most of the conformations confirmed pi-stacking interaction between hACE2 Tyr41 and Omicron RBD Tyr501, which has been regarded as one of the reasons that explains the higher viral load and infectivity of the N501Y-bearing SARS-CoV-2 variant.

Apart from the CoM distance method, which is the main point of discussion in this study, researchers have also exploited additional *in silico* methods, such as residue fluctuation, radius of gyration, solvent accessible surface area and free energy landscapes, in order to analyze the fundamental properties of SARS-CoV-2 proteins' interactions^{10,11} or evaluate the structural impact of selected mutations.¹²⁻¹⁴ Docking studies proved to be especially useful in selecting highly effective SARS-CoV-2 inhibitors. Stability of the formed complexes has been used as a prime criterion to evaluate the inhibitory potential of each candidate. Ahamad *et al.*¹⁰ found that anidulafungin has the same neutralizing capacity as the well-studied lopinavir. In another study, Ahamad *et al.*¹¹ evaluated the efficiency of several N-protein targeted antagonists and suggested 4E1RCat and TMCB as candidate drugs. MD simulations have also been used to study the impact of selected mutations. *In silico* findings that RBD and Heptad Repeat 1 mutations can impose major structural destabilization, affecting pre-binding protein structure, which may negatively impact current therapeutic efforts, have been presented in several papers.¹²⁻¹⁴

In some instances, using the average of the intermolecular CoM distance during the whole MD simulation,^{2,3} may give rise wrong conclusions related to the binding affinity change. The reason for this is the fact that molecules usually exhibit sudden and sharp local and global movements, one relative to another, before entering

the convergent state. In such cases, prior-convergent oscillations may easily suppress the impact of relative flat and convergent CoM distance amplitudes. Having them averaged during the course of the whole MD simulation, a wrong conclusion about the real direction of the affinity change may be derived.

To explain this situation better, let's take two random systems A and B, with a total of eight CoM distance snapshots [nm], such as the first five are prior-convergent samples and the last three convergent: A={4; 4.5; 3.9; 3.8; 3.5; 2.8; 2.75; 2.75} and B={3; 4; 4.5; 3; 3.2; 2.83; 2.82; 2.81}. By considering the integral systems' dynamics, upon the eight CoM distance snapshots, the average CoM distance in the system A is higher than the one in the system B (3.5 nm vs. 3.27 nm), which is interpreted in terms of reduced binding affinity between the units in system A in comparison to the binding affinity between the units in system B. However, the opposite of the previous conclusion is actually true, as the average CoM distance throughout the convergent state upon the last three snapshots in the system A is less than the one in system B (2.77 nm versus 2.82 nm).

An intuitive solution to this problem is to compute the average of the intermolecular CoM distance during the convergent phase only and neglect the non-convergent system's behavior. It is of crucial importance in the cases where the individual impact of a particular mutation or a combination of a few mutations need to be estimated, a situation in which the wild-type and mutant complex share very similar CoM distance plots.

2. Method overview

Let W be the wild-type heterodimer and M the mutant of W . W can be retrieved from the Protein Data Bank in.pdb format. Molecular visualization software, such as PyMol, can be used to mutate the wild-type heterodimer W to M . Initially, both systems, W and M , need to be well-prepared and energetically optimized within self and toward the solvent that will guarantee that the systems are stable enough to undergo the process of MD simulation. The details of systems' preparation steps are described in the section 3. The method is formally described in the next section (Figure 1).

2.1. Formal description of the method

The CoM of a monomer of n atoms at positions r_j and masses: m_1, m_2, \dots, m_n can be computed as:

$$com = \frac{\sum_{i=1}^n m_i r_i}{\sum_{i=1}^n m_i} \quad (1)$$

where com is an oscillating point in the time (t): $com(t)=(x(t),y(t),z(t),z(t))$.

Equation I can be applied to compute monomer [1] (M_1) and monomer [2] (M_2) CoM:

$$com_{M_1}(t) = (x_{M_1}(t), y_{M_1}(t), z_{M_1}(t)) \text{ and}$$

$com_{M_2}(t) = ((x_{M_2}(t), y_{M_2}(t), z_{M_2}(t)))$. Equation II can be used to compute the CoM distance between monomers M_1 and M_2 during the course of MD simulation.

$$d_{com}(t) = d_{M_1, M_2}(t) = \left((x_{M_1}(t) - x_{M_2}(t))^2 + (y_{M_1}(t) - y_{M_2}(t))^2 + (z_{M_1}(t) - z_{M_2}(t))^2 \right)^{\frac{1}{2}} \quad (II)$$

For the sake of simplicity, we use $d_{com,W}(t)$ and $d_{com,M}(t)$ to denote the CoM distance between monomers in the wild-type and mutant heterodimer.

At first, we use $d_{com}(t)$ to distinguish between non-convergent and convergent system's dynamics. During the non-convergent phase, monomers have not yet entered a mutually stable conformation, and large movements are likely to occur that will result in sharp $d_{com}(t)$ oscillations. On the other hand, once they have entered a mutually stable conformation, the CoM distance is preserved at a relatively constant level, resulting in smooth $d_{com}(t)$ transitions.

Given that t_{eq} is the earliest time point that marks the joint beginning of the convergent phase in both heterodimers, we compare average($d_{com,M}(t \geq t_{eq})$) against average($d_{com,W}(t \geq t_{eq})$), in order to draw a conclusion about the binding affinity change in comparative context, based on the fulfillment of condition (a), (b), or (c):

- If average($d_{com,M}(t \geq t_{eq})$) > average($d_{com,W}(t \geq t_{eq})$): Induced mutation(s) decrease intermolecular binding affinity;
- If average($d_{com,M}(t \geq t_{eq})$) < average($d_{com,W}(t \geq t_{eq})$): Induced mutation(s) increase intermolecular binding affinity;
- If average($d_{com,M}(t \geq t_{eq})$) \approx average($d_{com,W}(t \geq t_{eq})$): Induced mutation(s) do not substantially alter intermolecular binding affinity.

2.2. Method implementation in GROMCAS MD simulation software

The method can be implemented in GROMACS MD simulation software, using the following output files:

- .xtc* file: compressed MD trajectory file;
- .tpr* file: portable binary run input file that contains the initial structure, the topology and simulation parameters;
- .gro* file: that contains molecular structure in Gromos87 file format.

The first step is to call `gmx make_ndx` program to create separate index groups for the monomers in each

heterodimer. The program reads the complete heterodimer structure, provided by *.gro* file. For each monomer in the system, separate index files can be compiled, provided by the residues' range selection option *ri*, such as: *ri 1-597* (for monomer M_1) and *ri 598-791* (for monomer M_2). The program generates *.ndx* file, followed by *-o* output flag. Typical command use would be:

```
gmx make_ndx -f npt.gro -o index.ndx
```

Having split monomers into separate index groups (by default indexed as groups 18 and 19), `gmx distance` program can be used to compute the distance between monomers' CoM, during the course of the simulation. The following command computes and writes down the distance between monomers' CoM in *.xvg* file, having provided *.xtc* and *.tpr* files as input arguments and having selected corresponding monomers from the *.ndx* file:

```
gmx distance -f md.xtc -s md.tpr -n index.ndx -oall output_file.xvg -select 'com of group 18 plus com of group 19'
```

The obtained CoM distance results in *.xvg* format: $d_{com,W}$ (for the wild-type heterodimer) and $d_{com,M}$ (mutant heterodimer) that can be plotted in MS Excel. One can use the plot to identify the earliest time point t_{eq} , when both heterodimers enter stable conformation. We can identify the binding affinity impact of induced protein mutations, depending on which of the conditions (a), (b), or (c) becomes true.

3. In silico experiment: Systems preparation and MD simulation

For the purpose of the experiment, Protein Data Bank (<https://www.rcsb.org>) structure: 6M0J,¹⁵ was used as a wild-type molecular complex. 6M0J heterodimer (<https://www.rcsb.org/structure/6m0j>) includes two monomers, namely, chain A (hACE2 receptor, residues range: [19 – 615]) and chain E (SARS-CoV-2 S-protein RBD, residues range: [333 – 526]); N-acetyl-D-glucosamine ligands; and additional metal ions, such as zinc cations. Amino acids included in the 6M0J model represent the key interface of hACE2-RBD interactions.

PyMol software (<https://pymol.org/2/>, version 2.5.4) was used to clean up all non-protein content and mutate wild-type K417 (Lys417) in SARS-CoV-2 S-protein to Y417 (Tyr417). In spite of 3D molecule visualization, PyMol also enables easy content modification. PyMol mutagenesis tool was used to mutate wild-type K417 (Lys417) to Y417 (Tyr417) in the SARS-CoV-2 S-protein.

Both heterodimers, bearing K417/Y417 in the S-protein, followed equal preparation procedure. Heterodimers were dissolved under the SPC/E (simple point-charge/extended)

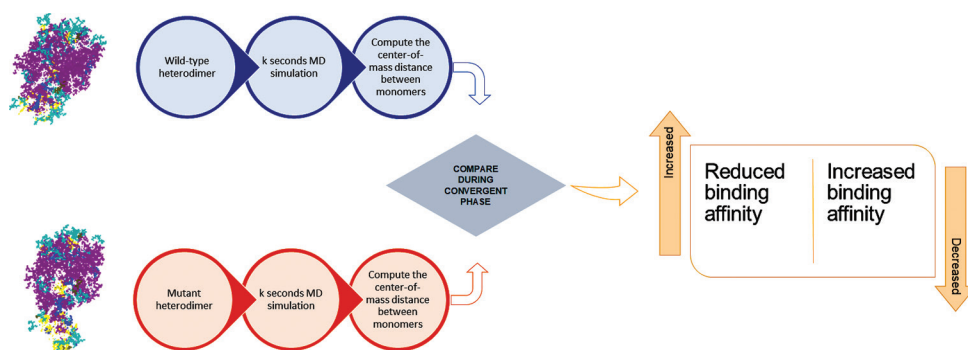


Figure 1. Visualization of the proposed method.

water model, having placed them and centered into a cubic box at 1 nm minimum distance from the edge of the box. Brooks *et al.*¹⁶ showed that Charmm27 all-atom force field was used for the purpose of simulation. Totally, 25 water molecules were substituted with 25 Na⁺ ions to bring up the systems to the neutral net charge. The systems were relaxed and optimized within-self applying the steepest descent energy minimization algorithm,¹⁷ until potential energy $E_{pot} < -10^5 \text{ kJmol}^{-1}$.

The purpose of 100-ps NVT equilibrium phase, controlled by V-rescale thermostat, was to bring the systems under the desired temperature of 310 K. V-rescale belongs to a sophisticated group of algorithms named thermostats and its role is to maintain a constant temperature level in the system throughout the process of MD simulation. The NVT equilibrium phase of 100-ps granted referent coupling pressure of 1 bar, assuming water isothermal compressibility equivalent to $4.45 \times 10^{-5} \text{ bar}^{-1}$ at $T = 310 \text{ K}$. Relaxed heterodimers were subjects to 50-ns MD simulation in GROMACS software.¹⁸

The aim of the *in silico* experiment was to evaluate the relative binding affinity change due to *K417Y* mutation in a comparative context: increased, decreased or no change, by measuring the CoM distance between the monomers in the common convergent state.

4. Results

Figure 2 shows the CoM distance between monomers in K417/Y417 heterodimers: $d_{com,K417}(t)$ and $d_{com,Y417}(t)$, during the course of 50-ns MD simulation. The substitution of positively charged Lysine(k) to polar, uncharged Tyrosine(y) at position 417 in the S-protein of SARS-CoV-2 may increase, decrease or have no substantial effect on S-protein-hACE2 binding affinity.

Following the method's considerations, we should first identify the beginning of the convergent state (t_{eq}). Both heterodimers, K417 (wild-type) and Y417 (mutant), enter relatively stable CoM distance amplitudes after 46.7 ns

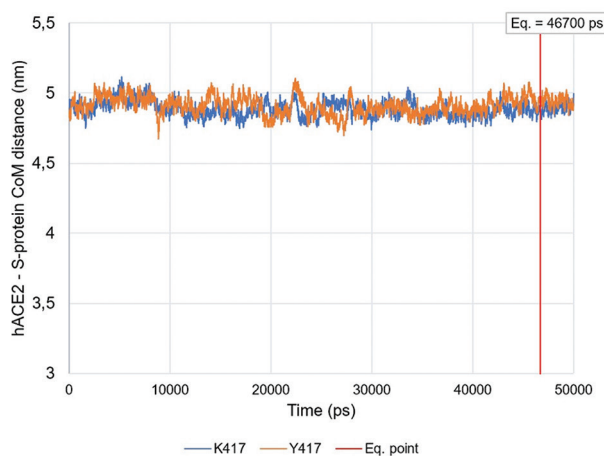


Figure 2. Evaluation of the impact of *K417Y* mutation by the means of $d_{com}(t)$ method.

(**Figure 2**), which is taken as an equilibrium point, $t_{eq} = 46.7$ ns. During the convergent phase $t = [46.7-50]$ ns, $d_{com,K417}(t)$ and $d_{com,Y417}(t)$ range $< 0.2 \text{ nm}$ (**Figure 2** and **Table 1**).

Throughout the convergent phase [46.7–50] ns, the mutant heterodimer Y417 exhibits higher intermolecular CoM distance than K417 wild-type: $d_{com,K417} = 4.943302115 \pm 0.037474346 \text{ nm}$ versus $d_{com,K417}(t) = 4.89718429 \pm 0.033584437 \text{ nm}$ (**Figure 2** and **Table 1**). The increase of the CoM distance in Y417 heterodimer relative to K417 favors partially reduced S-protein-hACE2 binding affinity in 6M0J heterodimer specifically.

Strictly speaking, and methodologically, condition (a) is fulfilled: $average(d_{com,Y417}(t \geq 46.7 \text{ ns})) = 4.943302115 \text{ nm} > 4.89718429 \text{ nm} = average(d_{com,K417}(t \geq 46.7 \text{ ns}))$ (**Table 1**), and the corresponding conclusion for partially reduced binding affinity between the monomers due to *K417Y* mutation is derived.

A key point in addition to the obtained results and derived conclusion is the fact that the analysis was

performed during the common convergent state in both heterodimers and not throughout the course of the entire simulation [0 – 50] ns, resembling the protocols in previous studies,^{2,3} potentially resulting in misleading conclusion related to the binding affinity change.

5. Discussion

Non-covalent interactions, specifically involving K417/Y417 residues, were analyzed, based on the relaxed, crystal pose K417/Y417 PDB structures, using the Ring 3.0 server¹⁹ (<https://ring.biocomputingup.it/>), for the following cutoff values: maximum ionic bond distance 4 Å, maximum hydrogen bond donor-acceptor distance 3.5 Å, maximum π - π stacking distance 4 Å, and Van der Waals radius intersection fraction of <0.01 Å.

It has been found that S-protein K417 participates in two interactions with hACE2 D30: an ionic bond/salt bridge and a hydrogen bond (Figure 3). Inside the S-protein, K417 forms two additional hydrogen bonds (K417-L455, K417-N422), and three van der Waals interactions of minor electrostatic impact involving D420, N422, and L455 (Figure 3). On the other hand, it has been found the S-protein Y417 forms only one hydrogen bond and two Van der Waals contacts with hACE2 D30 (Figure 3). Inside the S-protein, there is a hydrogen bond: Y417-N422 and Y417-D420 Van der Waals contact (Figure 3).

Residue interactions analysis in Ring 3.0 server¹⁹ showed that the major change, which happens due to the K417Y mutation, is the alteration of the much stronger salt bridge to a hydrogen bond, suggesting this change as a

Table 1. Analysis of $d_{com, K417}$ versus $d_{com, Y417}$ during the convergent phase [46.7–50] ns

Heterodimer	Average CoM distance (nm)	St. dev. CoM distance (nm)	Range (nm)
K417 (wild-type)	4.89718429	0.033584437	0.185
Y417 (mutant)	4.943302115	0.037474346	0.197

Abbreviations: st. dev.: Standard deviation; CoM: Center-of-mass.



Figure 3. K417/Y417 contacts analysis in RING 3.0. Indicators: red dashes denote salt bridge; blue dashes denote hydrogen bond; blue-gray dashes denote Van der Waals contacts.

major point of interest, which has been analyzed in terms of 50-ns MD simulation (Figure 4 and Table 2).

In K417 heterodimer, the salt bridge was formed between deprotonated carboxylic acid COO^- in D30 (aspartic acid, hACE2) and the positively charged ϵ -amino group NH_3^+ in K417 (Lysine, S-protein) (Figure 4). The salt bridge was changed to hydrogen bond in Y417 mutant, formed between D30 carboxylate ion and K417 phenolic hydroxyl group (-OH) (Figure 4).

Although the salt bridge is a k-fold stronger interaction than the hydrogen bond, it has been inspected for the occupancy of these interactions, as the overall impact of a strong but temporary interaction may be outcompeted by a weaker but permanent interaction(s).

Figure 4 shows the occupancy of D30-K417 salt bridge and D30-Y417 hydrogen bond per frame, during the course of MD simulation [0 – 50] ns. Binary coding scheme “1/0” is used to denote the presence/absence of a specific interaction, “1” for present and “0” for absent interaction (Figure 4). The salt bridge is present, if the distance between COO^- (D30) and NH_3^+ (K417) is <0.4 nm.²⁰ The module gmx distance was used to calculate the distance between COO^- (D30) and NH_3^+ (K417) per frame. The presence of the hydrogen bond was detected based on the geometric criteria for hydrogen bond formation: donor-acceptor distance (r_{DA}) <0.35 nm and hydrogen-donor-acceptor angle ($\angle had$) <30.²¹ The module gmx hbond was used for this purpose.

Table 2 summarizes the occupancy of the D30-K417 salt bridge and D30-Y417 hydrogen bond, during the course of the MD simulation $t = [0-50]$ ns and specifically during the convergent phase, $t \geq 46.7$ ns. In both cases, the occupancy of the salt bridge was higher than the occupancy of the hydrogen bond (Figure 4 and Table 2).

During the convergent phase ($t \geq 46.7$ ns) or the stabilized systems' dynamics, the salt bridge becomes a permanent intermolecular interaction with an occupancy = 98.5% (Table 2 and Figure 4), while the hydrogen bond shifts

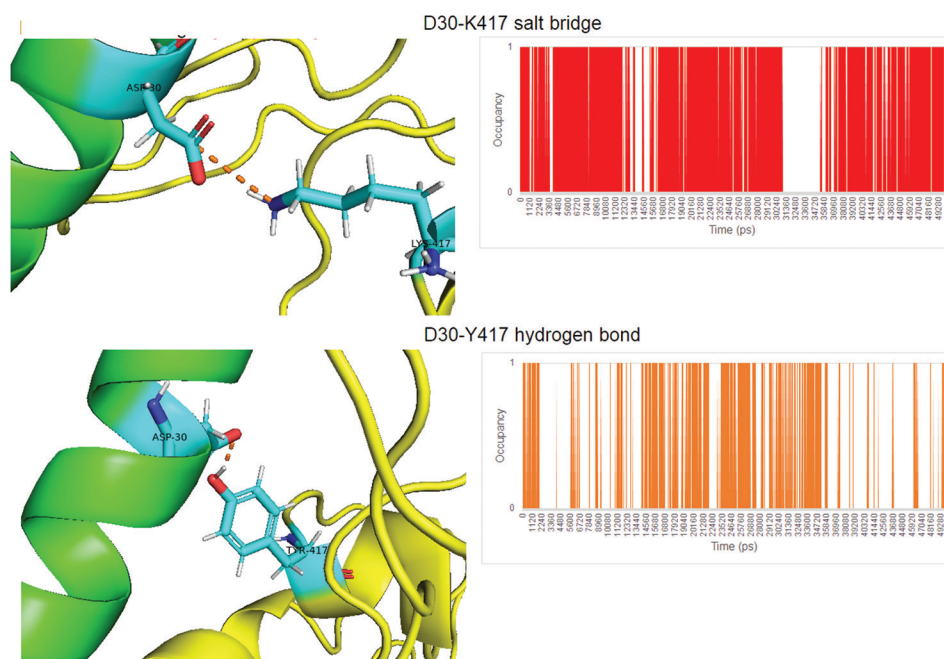


Figure 4. Visualization of mutation specific non-covalent interactions and their occupancy [0–50] ns.

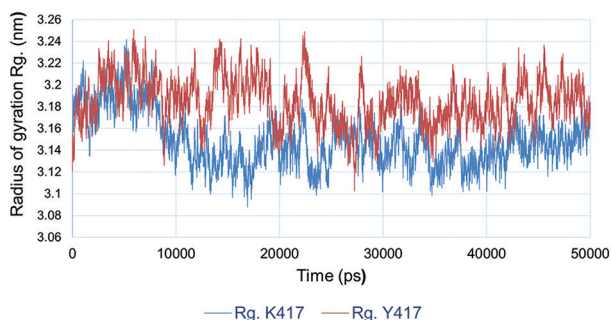


Figure 5. Radius of gyration.

to an interaction of a temporary character with an occupancy = 24.8% (Table 2 and Figure 4). The change of the strong and permanent salt bridge in *K417* wild-type heterodimer to a temporary hydrogen bond in *Y417* mutant, during the convergent phase, favors partial decrease of the binding affinity between SARS-CoV-2 S-protein and hACE2.

This conclusion is the same as the conclusion derived by the application of the CoM distance method, confirming the reliability of the proposed methodology.

The reduced binding affinity due to K417Y substitution will also favor minor complex destabilization, which has been proved in terms of the increased radius of gyration (Table 2 and Figure 5). The average radius of gyration in Y417 complex equals to 3.1852 ± 0.0217 nm, compared to 3.1488 ± 0.0242 nm in K417 (Table 2 and Figure 5).

Table 2. Occupancy of mutation-specific interactions in heterodimers and radius of gyration analysis

Heterodimer	<i>K417</i> (wild-type)	<i>Y417</i> (mutant)
Occupancy [0–50] ns	D30-K417 salt bridge 77.9%	D30-Y417 hydrogen bond 41.9%
Occupancy [46.7–50] ns	98.5%	24.8%
Radius of gyration (average±standard deviation)	3.1488 ± 0.0242 nm	3.1852 ± 0.0217 nm

Rather than evaluating the strict impact of *K417Y* mutation, which may require MD simulation longer than 50 ns, the experiment, experimental design and results reported in this study serve the illustrative purpose for accurate application of the CoM distance method.

Even though both systems enter a steady state after 46.7 ns or a total of 3.3 ns of assumed convergent system behavior have been observed, monitoring a much longer convergent state would be a better guarantee for not being trapped in a local well.

6. Conclusion

This study depicts the application of the CoM distance method. The CoM distance analysis should be limited to the common convergent state in both systems, which guarantees accurate affinity analysis. The application of the method can be further expanded to artificial intelligence-based protein structure databases, complexes modeled

with protein-protein docking, and affinity testing using the proposed method.

Acknowledgments

None.

Funding

None.

Conflict of interest

The author declares no competing interest.

Author contributions

This is single-authored article.

Ethics approval and consent to participate

Not applicable.

Consent for publication

Not applicable.

Availability of data

Data used in this work are available from the corresponding author on reasonable request.

References

- Stojanov D. Structural implications of SARS-CoV-2 surface glycoprotein N501Y mutation within receptor-binding domain [499-505]-computational analysis of the most frequent Asn501 polar uncharged amino acid mutations. *Biotechnol Biotechnol Equip.* 2023;37(1):2206492. doi: 10.1080/13102818.2023.2206492
- Ibrahim MA, Abdelrahman AH, Mohamed TA, et al. In silico mining of terpenes from red-sea invertebrates for SARS-CoV-2 main protease (M^{pro}) inhibitors. *Molecules.* 2021;26(7):2082. doi: 10.3390/molecules26072082
- Kumar R, Murugan NA, Srivastava V. Improved binding affinity of omicron's spike protein for the human angiotensin-converting enzyme 2 receptor is the key behind its increased virulence. *Int J Mol Sci.* 2022;23(6):3409. doi: 10.3390/ijms23063409
- Carter C, Airas J, Parish CA. Atomistic insights into the binding of SARS-CoV-2 spike receptor binding domain with the human ACE2 receptor: The importance of residue 493. *J Mol Graph Model.* 2023;118:108360. doi: 10.1016/j.jmgm.2022.108360
- Tian F, Tong B, Sun L, et al. N501Y mutation of spike protein in SARS-CoV-2 strengthens its binding to receptor ACE2. *Elife.* 2021;10:e69091. doi: 10.7554/eLife.69091
- Godschalk F, Genheden S, Söderhjelm P, Ryde U. Comparison of MM/GBSA calculations based on explicit and implicit solvent simulations. *Phys Chem Chem Phys.* 2013;15(20):7731-7739. doi: 10.1039/C3CP00116D
- Stojanov D. Phylogenicity of B.1.1.7 surface glycoprotein, novel distance function and first report of V90T missense mutation in SARS-CoV-2 surface glycoprotein. *Meta Gene.* 2021;30:100967. doi: 10.1016/j.mgene.2021.100967
- Stojanov D. Data on multiple SARS-CoV-2 surface glycoprotein alignments. *Data Brief.* 2021;38:107414. doi: 10.1016/j.dib.2021.107414
- Deng JH, Luo J, Mao YL, et al. π - π stacking interactions: Non-negligible forces for stabilizing porous supramolecular frameworks. *Sci Adv.* 2020;6(2):eaax9976. doi: 10.1126/sciadv.aax9976
- Ahamad S, Ali H, Secco I, Giacca M, Gupta D. Anti-fungal drug anidulafungin inhibits SARS-CoV-2 spike-induced syncytia formation by targeting ACE2-spike protein interaction. *Front Genet.* 2022;13:866474. doi: 10.3389/fgene.2022.866474
- Ahamad S, Gupta D, Kumar V. Targeting SARS-CoV-2 nucleocapsid oligomerization: Insights from molecular docking and molecular dynamics simulations. *J Biomol Struct Dyn.* 2022;40(6):2430-2443. doi: 10.1080/07391102.2020.1839563
- Ahamad S, Hema K, Ahmad S, Kumar V, Gupta D. Insights into the structure and dynamics of SARS-CoV-2 spike glycoprotein double mutant L452R-E484Q. *Biotech.* 2022;12(4):87. doi: 10.1007/s13205-022-03151-0
- Ahamad S, Hema K, Gupta D. Structural stability predictions and molecular dynamics simulations of RBD and HR1 mutations associated with SARS-CoV-2 spike glycoprotein. *J Biomol Struct Dyn.* 2022;40(15):6697-6709. doi: 10.1080/07391102.2021.1889671
- Ahamad S, Kanipakam H, Gupta D. Insights into the structural and dynamical changes of spike glycoprotein mutations associated with SARS-CoV-2 host receptor binding. *J Biomol Struct Dyn.* 2022;40(1):263-275. doi: 10.1080/07391102.2020.1811774
- Lan J, Ge J, Yu J, et al. Structure of the SARS-CoV-2 spike receptor-binding domain bound to the ACE2 receptor. *Nature.* 2020;581(7807):215-220. doi: 10.1038/s41586-020-2180-5
- Brooks BR, Brucoleri RE, Olafson BD, States DJ,

- Swaminathan SA, Karplus M. CHARMM: A program for macromolecular energy, minimization, and dynamics calculations. *J Comput Chem*. 1983;4(2):187-217.
doi: 10.1002/jcc.540040211
17. Curry HB. The method of steepest descent for non-linear minimization problems. *Q Appl Math*. 1944;2(3):258-261.
doi: 10.1090/qam/10667
18. Abraham MJ, Murtola T, Schulz R, *et al*. GROMACS: High performance molecular simulations through multi-level parallelism from laptops to supercomputers. *SoftwareX*. 2015;1-2:19-25.
doi: 10.1016/j.softx.2015.06.001
19. Clementel D, Del Conte A, Monzon AM, *et al*. RING 3.0: Fast generation of probabilistic residue interaction networks from structural ensembles. *Nucleic Acids Res*. 2022;50(W1):W651-W656.
doi: 10.1093/nar/gkac365
20. Kumar S, Nussinov R. Close-range electrostatic interactions in proteins. *ChemBioChem*. 2002;3(7):604-617.
doi: 10.1002/1439-7633(20020703)3:7<604::AID-CBIC604>3.0.CO;2-X
21. Baker EN, Hubbard RE. Hydrogen bonding in globular proteins. *Prog Biophys Mol Biol*. 1984;44(2):97-179.
doi: 10.1016/0079-6107(84)90007-5